JOURNAL OF MATERIALS SCIENCE 32 (1997) 989–996

A study on the nickel-rich ternary Ti–Ni–Al shape memory alloys

S. F. HSIEH, S. K. WU
Institute of Materials Science and Engineering, National Taiwan University, Taipei, Taiwan 106, Republic of China

The transformation sequence and hardening effects of 400 °C aged $Ti_{47.5}Ni_{50.65}Al_{1.85}$ and $Ti_{49.5}Ni_{50.13}Al_{0.37}$ shape memory alloys have been investigated by electrical resistivity tests, internal friction measurements, hardness tests and TEM observations. Both solution hardening and precipitation hardening are found to occur in these alloys. The hardening effects of $Ti_{47.5}Ni_{50.65}Al_{1.85}$ alloy are obvious and much higher than those of $Ti_{49.5}Ni_{50.13}Al_{0.37}$ alloy due to the former having the larger Ni/Ti ratio and a higher Al solute content in its matrix. The transformation sequence of 400 °C aged $Ti_{47.5}Ni_{50.65}Al_{1.85}$ alloy shows B2↔R-phase only for an ageing time of more than 10 h and that of 400 °C aged $Ti_{49.5}Ni_{50.13}Al_{0.37}$ alloy shows the sequence B2↔R-phase↔B19′ or B2↔R-phase with different ageing times. All of these characteristics are associated with $Ti_{11}Ni_{14}$ precipitates during the ageing process. These aged Ti–Ni–Al alloys exhibit very good shape memory effects, in which the maximal shape recovery occurs at the peak of hardness.

1. Introduction

The binary TiNi alloys display several solid-state phase transformations, including B2↔B19′, B2↔R-phase↔B19′ and B2↔R-phase transformations. There are many factors which cause the premartensite R-phase to appear in TiNi alloys, such as increasing Ni content [1–3], ageing Ni-rich alloys [4, 5], annealing at low temperatures immediately after cold working [4], substituting a third element [5, 6], and conducting thermal cycling [7–9], etc. Thus, the R-phase premartensite can appear prior to the martensitic transformation in the aged $Ti_{49}Ni_{51}$ alloy. This has been investigated by many authors [10–15], mainly by use of electrical resistivity tests, transmission electron microscopy (TEM) observations and internal friction measurements. In these reported studies, the transformation temperatures of R-phase and martensite are strongly affected by the ageing time and temperature due to $Ti_{11}Ni_{14}$ precipitates [10, 13–15]. As for ternary Ti–Ni–Al shape memory alloys, the aged Ti-rich $Ti_{59.4}Ni_{38.7}Al_{1.9}$ alloy has a large temperature separation between the R-phase and martensitic transformations [16]. TEM studies of the R-phase transformation of this Ti–Ni–Al alloy have also been investigated [17, 18]. However, transformation characteristics of Ni-rich Ti–Ni–Al alloys have yet to be reported. In this study, solution hardening and precipitation hardening are found to occur in Ni-rich Ti–Ni–Al aged alloys. The effect of the added aluminium on the precipitation hardening, transformation sequence, shape recovery and microstructure in these alloys are also investigated.

2. Experimental procedure

The conventional tungsten arc melting technique was employed to prepare alloys $Ti_{49.5}Ni_{50.13}Al_{0.37}$ (alloy A) and $Ti_{47.5}Ni_{50.65}Al_{1.85}$ (alloy B) (in atomic percent) in accordance with $Ti_{50}Ni_{50}$–$Ni_{63}Al_{37}$ pseudo-binary phase diagram, i.e. $(Ti_{50}Ni_{50})_{99}(Ni_{63}Al_{37})_1$ for the former alloy and $(Ti_{50}Ni_{50})_{95}(Ni_{63}Al_{37})_5$ for the latter alloy. Here, $Ni_{63}Al_{37}$ alloy also exhibits a thermoelastic martensitic transformation with the M_S temperature at -10 °C [19]. Titanium (purity 99.7%), nickel (purity 99.9%) and aluminium (purity 99.99%), totalling approximately 100 g, were melted and remelted at least six times in an argon atmosphere. Pure titanium buttons were also melted and used as a getter. The mass loss during the melting was negligibly small. The as-melted button was homogenized at 1000 °C for 72 h and cooled in a furnace. Specimens for electrical resistivity tests, shape memory effects (size: 50 mm × 1 mm × 1 mm), hardness tests (size: 5 mm × 3 mm × 3 mm) and internal friction measurements (size: 110 mm × 4 mm × 1 mm) were carefully cut from the homogenized button by a low speed diamond saw, sealed in evacuated quartz tubes, annealed at 850 °C for 2 h and then quenched in water. These are solution-treated (ST) specimens. Then they were isothermally aged in a salt bath at 400 °C for 1 to 400 h followed by quenching in water.

The martensitic and premartensitic transformation temperatures were measured by using a four-probe electrical resistivity measurement technique. Measurements were carried out at temperatures ranging from -196 to $+100$ °C. The hardness test was carried out

0022–2461

by using a micro-Vickers tester with 500 g load at room tempertaure. For each specimen, the average hardness value was determined from at least five test readings. The shape recovery measurement was performed as described earlier by Lin and Wu [20]. Internal friction (IF) measurements were carried out using a SINKU-RIKO 1500-M/L series inverted torsion pendulum in the temperature range of -196 to $+100\,^{\circ}C$. The temperature rate was precisely controlled at $2\,^{\circ}C\,min^{-1}$ and the test frequency was around 1 Hz. The recording of data was completely automatic; calculation and plots of IF and frequency f (shear modulus) versus temperature were performed on a digital computer.

TEM specimens were prepared by electropolishing at $0\,^{\circ}C$ with an electrolyte consisting of 20% H_2SO_4 and 80% CH_3OH by volume. The applied voltage was 20 V. Electron diffraction and TEM microstructure were carried out using a Jeol-100CXII microscope operated at 100 kV and equipped with a conventional double tilting stage. A quantitative analysis was performed by using a Jeol -4000FX microscope equipped with an energy dispersive X-ray (EDX) system.

3. Experimental results

Fig. 1a–g shows the experimental results of electrical resistivity versus temperature for alloy A aged at $400\,^{\circ}C$ for 0, 1, 10, 50, 120, 240 and 400 h, respectively. The notation for the determination of transformation temperatures on these curves, including T_R, T_R^*, M_S, M_f, A_S and A_f, follows the notation demonstrated by Hwang *et al.* [21]. Derived from Fig. 1, transformation temperatures versus ageing time is plotted in Fig. 2. Fig. 2 shows that martensitic and R-phase transformation temperatures are all affected by the ageing time. Among them, M_S and M_f temperatures decrease slowly in the early ageing, depress sharply after 50 h ageing and reach a minimum at 120 h, and then increase with further ageing.

Fig. 3a–e shows the experimental results of electrical resistivity versus temperature for alloy B aged at $400\,^{\circ}C$ for 0, 50, 120, 240 and 400 h, respectively. Only the R-phase transformation can be seen in Fig. 3. As shown in Fig. 3, transformation temperatures of M_S, M_f, A_S and A_f are all below the liquid nitrogen temperature and therefore cannot be detected on both cooling and heating curves.

Fig. 4a and b shows plots of frequency f (shear modulus) and IF versus temperature for $400\,^{\circ}C \times 50$ h aged alloy B. In Fig. 4b, there is one peak P_C at $-37\,^{\circ}C$ on cooling and one sharp peak P_H at $-31\,^{\circ}C$ on heating. Both peaks which correspond to the minima of frequency f, shown in Fig. 4a, indicate minima of shear modulus G. Compared with the results of Figs 3 and 4, we are sure that these peaks are associated with the R-phase transformation. The peak P_R appearing at $-80\,^{\circ}C$ and not corresponding to the minimum of frequency f is proposed to be a relaxation peak [22, 23]. The relaxation peak is associated with the interaction of dislocations and point defects [23] and is independent of the martensitic and premartensitic transformations [14]. From Figs 1, 3 and 4, one can find that the occurrence of R-phase premartensitic transformation can be enhanced by a little Al added to Ni-rich TiNi alloys. At the same time, the R-phase transformation temperatures are also affected by the ageing time. T_R and T_R^* temperatures increase significantly during early ageing 50–120 h, and then remain nearly constant when aged further.

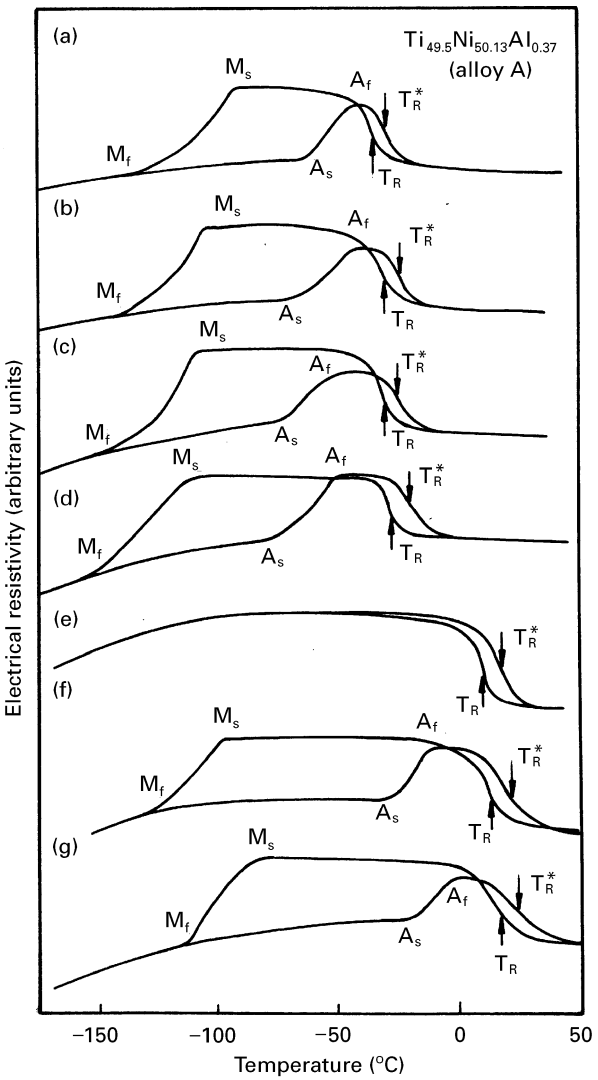

Figure 1 Electrical resistivity versus temperature of $Ti_{49.5}Ni_{50.13}Al_{0.37}$ alloy (alloy A) aged at $400\,^{\circ}C$ for (a) 0 h (as solution-treated, ST) (b) 1 h, (c) 10 h, (d) 50 h, (e) 120 h, (f) 240 h and (g) 400 h.

Fig. 5a, b and c show TEM bright field images of alloy A aged at $400\,^{\circ}C$ for 240 h and alloy B aged at $400\,^{\circ}C$ for 50 and 240 h, respectively. The occupied volume of precipitates in Fig. 5a, b and c is about 2–3%, 15% and 15%, respectively. The selected area diffraction pattern (SADP) of Fig. 5b is shown in Fig. 5d in which the foil normal is parallel to the $\langle 1\,1\,1\rangle_{B2}$ direction. In Fig. 5d, 1/7 spots can be observed along $\langle \bar{3}\,2\,1\rangle_{B2}$. This feature indicates that the precipitates are similar to those observed in the aged Ni-rich $Ti_{49}Ni_{51}$ alloy [24, 25] and therefore are identified to be the $Ti_{11}Ni_{14}$ phase. In Fig. 5a and b, $Ti_{11}Ni_{14}$ precipitates are oval plates and do not coarsen easily after a long ageing time. The interfaces of $Ti_{11}Ni_{14}$ precipitates and B2 matrix may be either semi-coherent or non-coherent. These results indicate that the Al

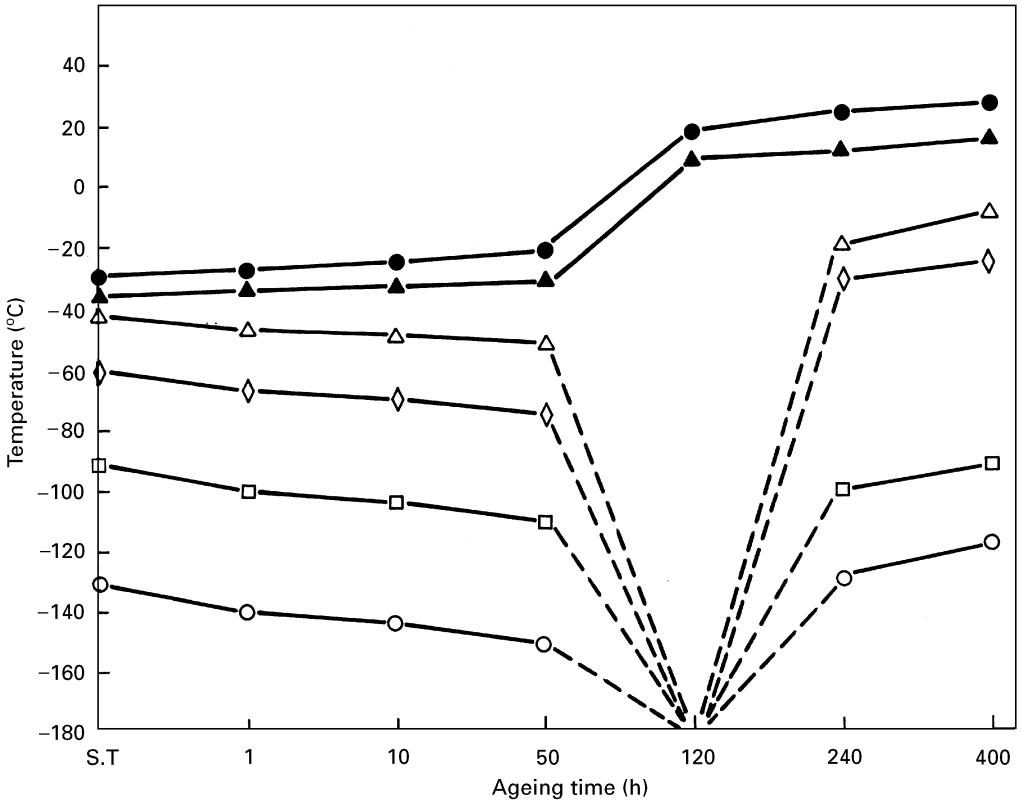

Figure 2 Transformation temperatures of M_s (□), M_f (○), A_s (◇), A_f (△) T_R (▲) and T_R^* (●) versus ageing time for $Ti_{49.5}Ni_{50.13}Al_{0.37}$ alloy (alloy A) aged at 400 °C.

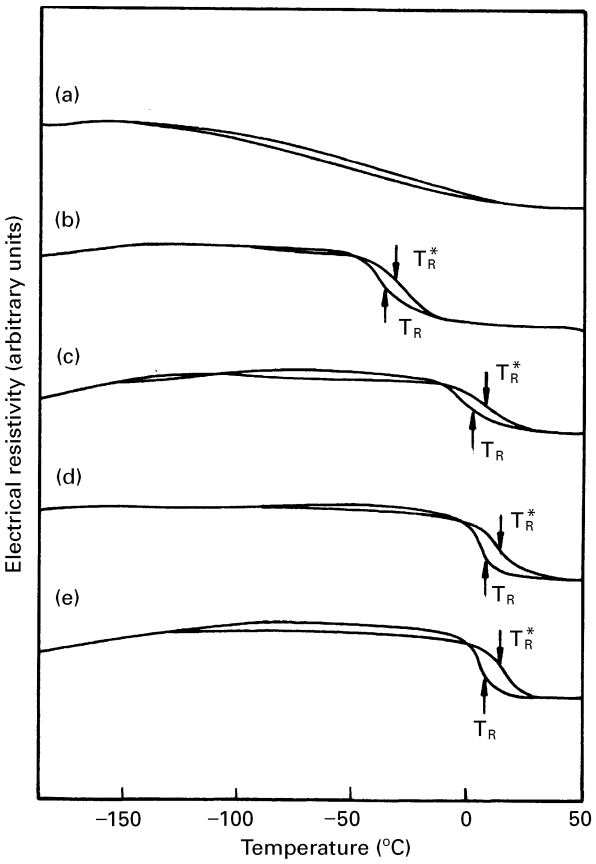

Figure 3 Electrical resistivity versus temperature of $Ti_{47.5}Ni_{50.65}Al_{1.85}$ alloy (alloy B) aged at 400 °C for (a) 0 h (ST), (b) 50 h, (c) 120 h, (d) 240 h and (e) 400 h.

added to Ni-rich TiNi alloys can impede the precipitates' growth during the course of ageing.

Fig. 6a and b shows EDX spectra (taken on a Jeol — 4000 FX microscope) of precipitates in alloy B aged at 400 °C for 50 and 240 h, respectively. The composition of the precipitates detected is about 1.66% Al, 54.21% Ni and 44.13% Ti (in at %) for both aged specimens. These results indicate that aluminium is soluted into $Ti_{11}Ni_{14}$ precipitates (1.66% Al) and that in the matrix 1.85% Al are present in the aged alloy B.

Fig. 7 shows H_V hardness values versus ageing time of alloys A and B after 400 °C ageing. From Fig. 7, it can be seen that the hardness continuously increases with increasing ageing time, reaches a maximum at 50 and 120 h for alloy B and alloy A, respectively, and then decreases with further ageing. For alloy B, the curve shown in Fig. 7 is obviously characteristic of $Ti_{11}Ni_{14}$ precipitation hardening during early ageing up to 50 h. Thereafter, the interface between parent phase and precipitates will gradually lose its coherence and the hardness will decrease. The solution-treated specimens of alloy B contain much more solid-soluted Al in the matrix than alloy A, therefore, the hardness of the former alloy should be higher than that of the latter one. Simultaneously, alloy B has the higher precipitation hardening effect compared to alloy A because the volume of precipitates in alloy B is much higher.

Fig. 8 shows the results of shape recovery measurements for the specimens of Fig. 7. In Fig. 8, the shape recovery effect increases with increasing ageing time,

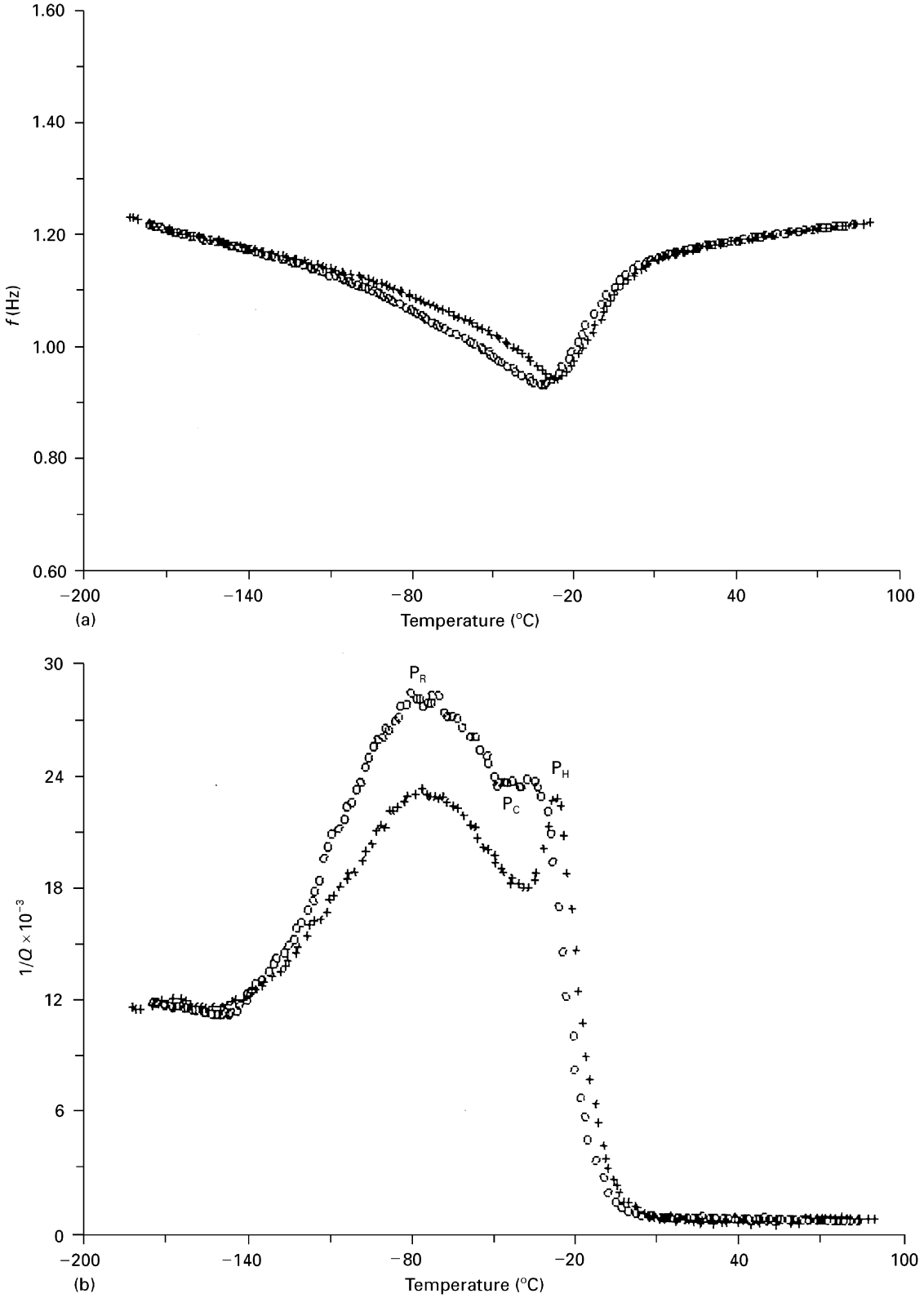

Figure 4 (a) Frequency *f*, (b) internal friction versus temperature for the $Ti_{47.5}Ni_{50.65}Al_{1.85}$ alloy (alloy B) aged at 400 °C × 50 h. Peaks P_C and P_H are associated with the R-phase transformation. P_R peak is a relaxation one. Key: + heating; ○ cooling.

reaches 100% at 50 h ageing for alloy B and at 120 h ageing for alloy A, and then decreases with further ageing. For alloy B, the early aged specimens (ageing time ≤ 10 h) have no shape recovery due to transformation temperatures below the liquid nitrogen temperature. Compared with Figs 7 and 8, one can find that the specimen having peak hardness has the maximal shape recovery.

4. Discussion

4.1. Transformation sequence of $Ti_{49.5}Ni_{50.13}Al_{0.37}$ and $Ti_{47.5}Ni_{50.65}Al_{1.85}$ alloys

It is well known that the R-phase transformation can appear prior to the martensitic transformation when the M_S point of TiNiX alloys is depressed. Figs 1 and 2 show that the transformation sequence of aged alloy

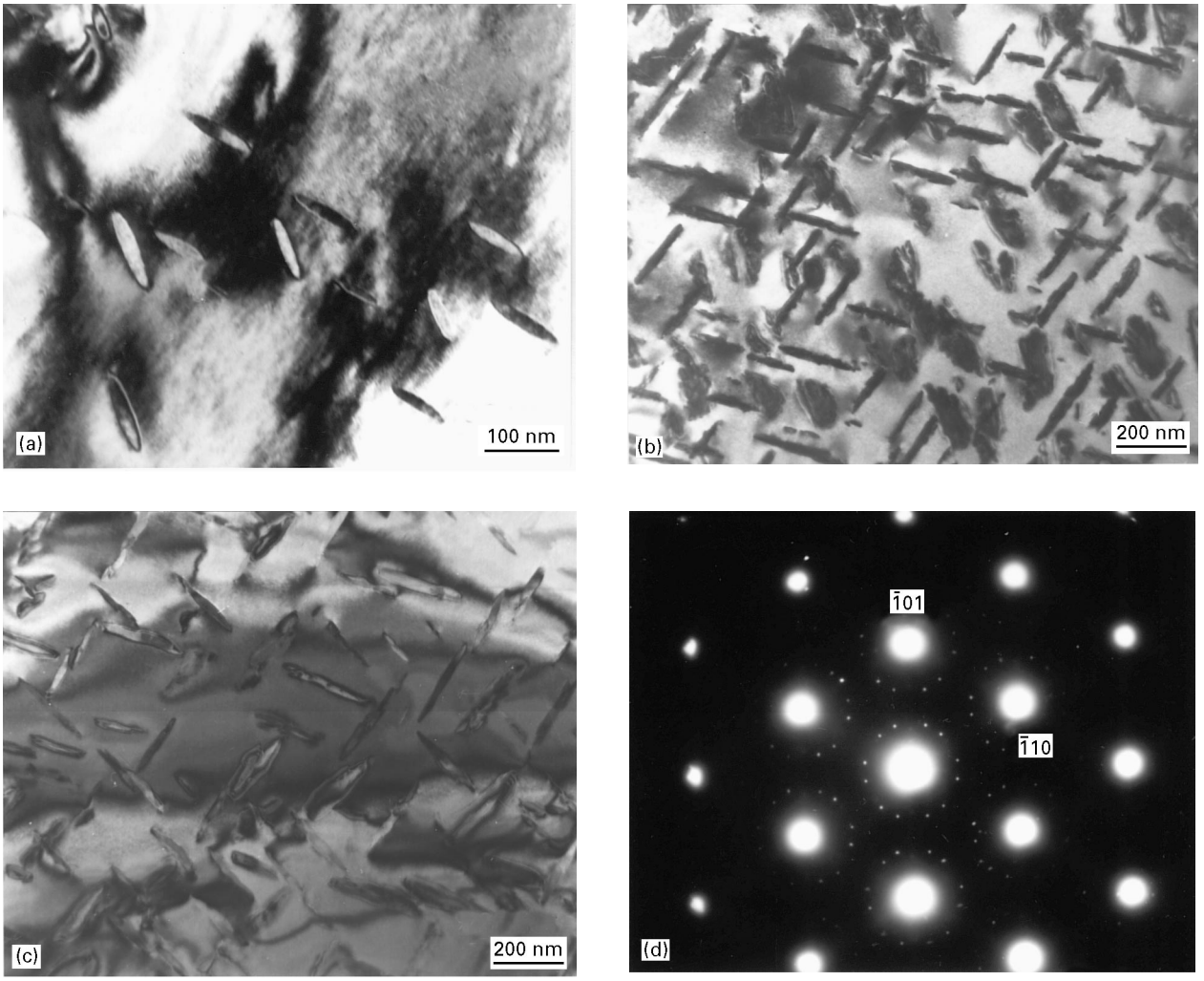

Figure 5 (a) TEM bright-field image of $Ti_{49.5}Ni_{50.13}Al_{0.37}$ alloy (alloy A) aged at 400 °C × 240 h, (b) TEM bright-field image of $Ti_{47.5}Ni_{50.65}Al_{1.85}$ alloy (alloy B) aged at 400 °C × 50 h, (c) the same as (b), but for 240 h, (d) SADP of (b), the zone axis is $[1\,1\,1]_{B2}$.

A proceeds upon cooling as B2 → R-phase → B19′ martensite in the early period of 50 h ageing, and then as B2 → R-phase at 120 h ageing due to the M_S being depressed below the liquid nitrogen temperature. For further ageing, the sequence of B2 → R-phase → B19′ can be obtained again. The transformation sequences as mentioned above are closely related to $Ti_{11}Ni_{14}$ precipitates. This is because coherent stresses induced by coherent boundaries between precipitates and matrix can effectively depress the martensitic transformation and enhance the R-phase transformation. This feature is similar to that reported in 400 °C aged $Ti_{49.2}Ni_{50.8}$ alloy [15, 22]. Note that, for the same 400 °C ageing, the maximal hardness occurs at 50 h for $Ti_{49.2}Ni_{50.8}$ alloy [15], but at 120 h for alloy A. This means that the small Al additions in Ni-rich TiNi alloy can retard the growth rate of precipitates during ageing due to the fact that coarsening of precipitates can destroy coherent boundaries.

Figs 3 and 4 show that the transformation sequence of aged alloy B is B2 → R-phase for ageing times of more than 10 h. Obviously, 1.85 at % Al soluted in Ni-rich TiNi alloy can significantly depress the martensitic transformation. This feature is similar to Ti–Ni–Fe ternary alloys in which only B2 → R-phase can be observed in more than 3% Fe added Ti–Ni–Fe alloys [21]. It is reported that the frequency f (shear modulus) of the R-phase transformation in 300–600 °C aged $Ti_{49}Ni_{51}$ alloy has a deep minimum frequency [11]. This phenomenon also occurs in aged alloy B, as shown in Fig. 4a. Eckelmeyer [2] and Edmonds and Hwang [16] studied the Al added Ti-rich TiNi alloys and found their M_S temperatures decrease and that the R-phase appears over a wide temperature range. They attributed this feature to the difference of the free energy change between R-phase and martensite due to the substitution of aluminium element in TiNi alloys. We suggest that the same reason can also apply to the Ni-rich Ti–Ni–Al alloys, such as the feature of alloy B shown in Fig. 3.

4.2. Hardening effects

Fig. 7 shows both solution hardening and precipitation hardening occurring in aged alloys A and B. It is reported that the Ni-rich $Ti_{48.5}Ni_{50.5}Al_{1.0}$ alloy aged at 400–600 °C also exhibits precipitation hardening [26]. From Fig. 7, it can be seen that the solution hardening of alloy B is much higher than that of alloy A. This feature is closely related to the amount of Ni

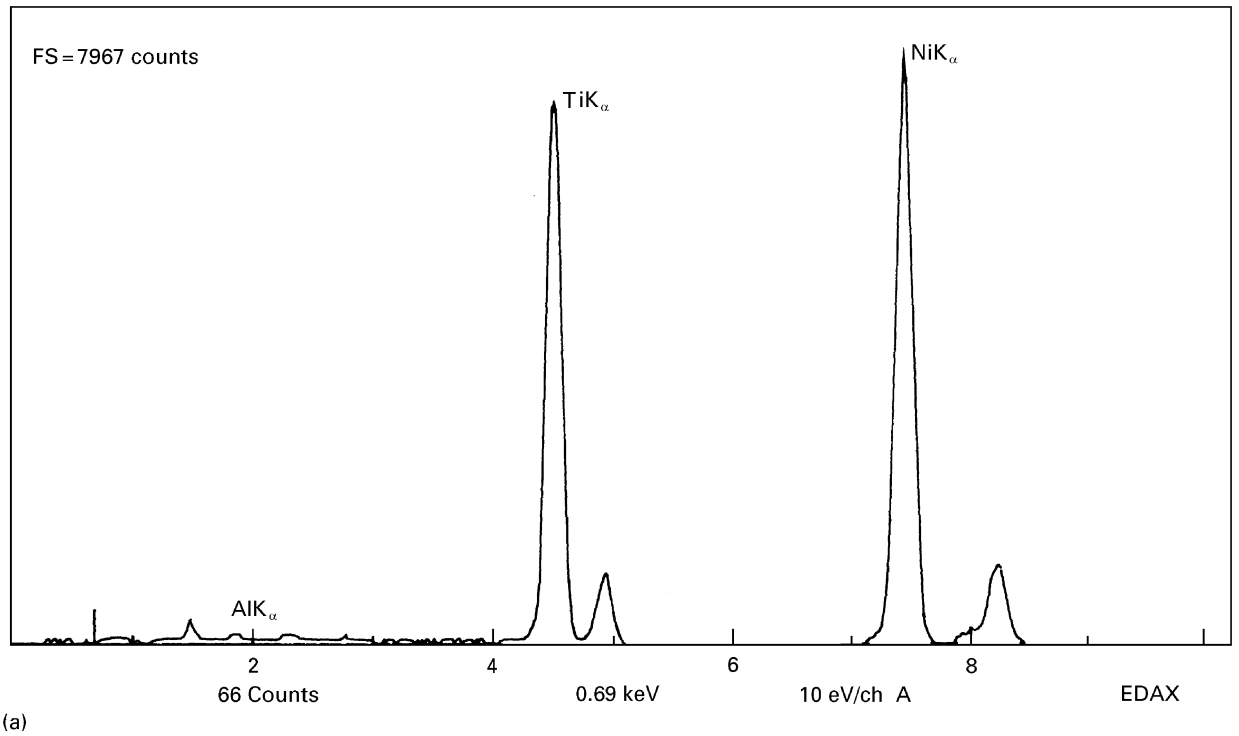

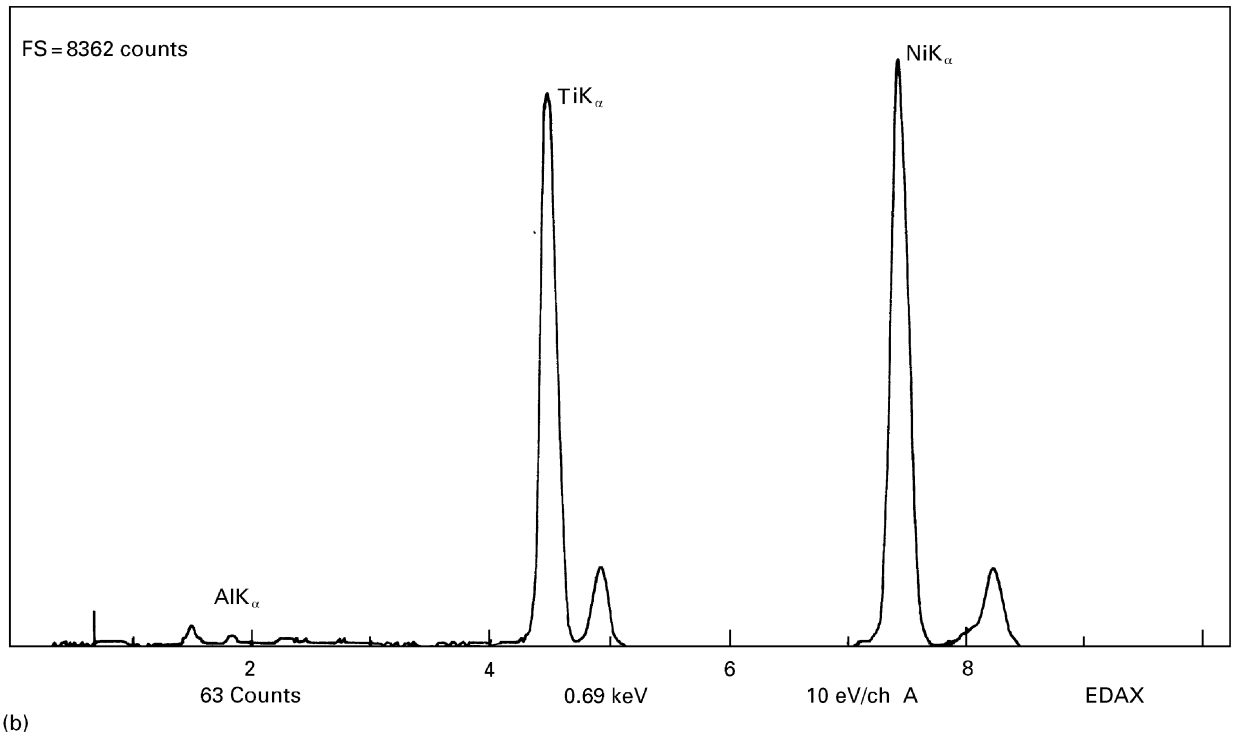

Figure 6 EDX spectra of precipitates for $Ti_{47.5}Ni_{50.65}Al_{1.85}$ alloy (alloy B) aged at 400 °C for (a) 50 h and (b) 240 h. The composition is identified as 1.66% Al, 54.21% Ni and 44.13% Ti (in at %).

and Al atoms in solid solution in these alloys. The effect of Ni composition on the hardness of non-stoichiometric TiNi binary alloys solution-treated at 1000 °C has shown that the larger Ni/Ti ratio has the higher hardness [27]. We suggest that the same effect may also occur in the solution-treated alloys of this study in which the Ni/Ti ratios are 1.013 and 1.066 for alloy A and alloy B, respectively. In addition to the Ni/Ti ratio, aluminium in solid solution in Ti–Ni–Al alloys can also affect the solution hardening. From Fig. 6, we can see Al atoms are solid-soluted in the matrix and in precipitates simultaneously during the precipitation hardening process. At the same time, Fig. 6 also indicates that the content of aluminium soluted in the matrix is similar to that of the precipitates for aged Ti–Ni–Al alloys. Therefore, the solution hardening effect induced by the soluted Al atoms remains during the ageing process. From the fact that more Al atoms are soluted in alloy B than in alloy A, the hardness of aged alloy B should always be larger than that of aged alloy A, as shown in Fig. 7.

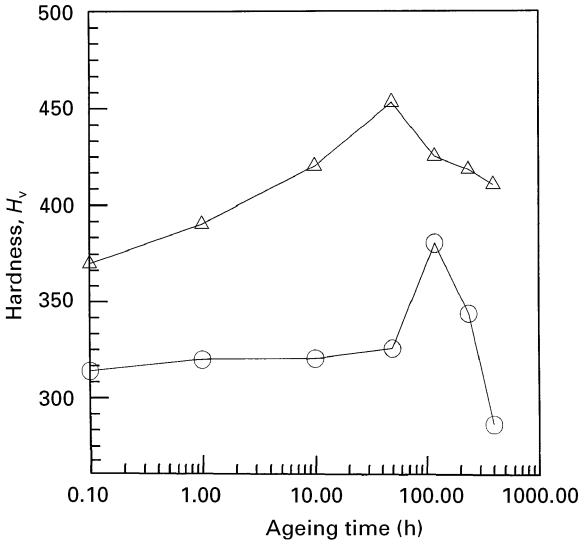

Figure 7 Hardness versus ageing time of 400 °C aged alloys $Ti_{49.5}Ni_{50.13}Al_{0.37}$ (alloy A) (○) and $Ti_{47.5}Ni_{50.65}Al_{1.85}$ (alloy B) (△).

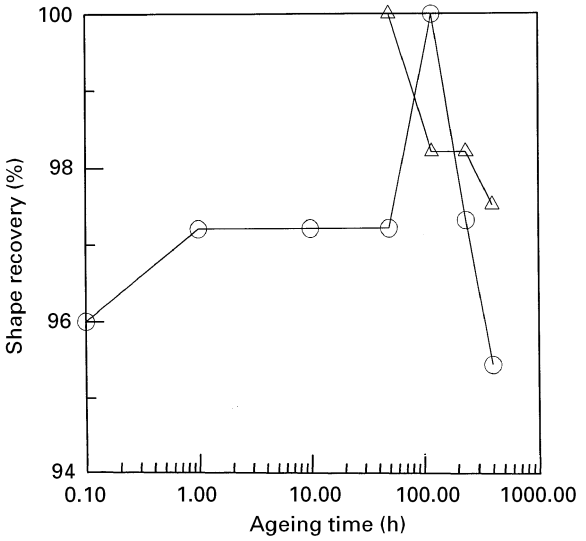

Figure 8 Shape memory effect (in terms of shape recovery, %) versus ageing time of 400 °C aged alloys $Ti_{49.5}Ni_{50.13}Al_{0.37}$ (alloy A) (○) and $Ti_{47.5}Ni_{50.65}Al_{1.85}$ (alloy B) (△).

Fig. 7 also indicates that the precipitation hardening of alloy A is not obvious during the early stages of 50 h ageing. This phenomenon can be attributed to the fact that alloy A has the lower Ni/Ti ratio and fewer solid-soluted Al atoms. For the low Ni/Ti ratio (approaching one), the nucleus number of $Ti_{11}Ni_{14}$ precipitates should be low. For the solid-soluted Al atoms, we suggest that Al atoms solid-soluted in TiNi alloy can retard the growth of precipitates. It is reported that the diffusion coefficients of minority atoms, such as B, Be, Si, Fe in the amorphous alloy $Ti_{60}Ni_{40}$ have been affected in the temperature range 300–420 °C [28]. At the same time, the diffusivity in ordered alloys can be affected by various jump mechanisms associated with different atomic binding energies and jump frequencies [29]. The diffusivity of Ti and Ni in the Ni-rich Ti–Ni–Al alloys should be affected by the fact that the atomic size and chemical affinity between Al and Ti, and that between Al and Ni should change the atomic binding energy in these alloys. Therefore, the growth rate of $Ti_{11}Ni_{14}$ precipitates in Ti–Ni–Al alloys should be different from that in TiNi binary alloys. From Fig 5 and Section 4.1, we find that the soluted Al atoms in Ti–Ni–Al alloy will retard the growth rate of $Ti_{11}Ni_{14}$ precipitates during the ageing process. Thus, we conclude that alloy A has slower nucleation and growth rates of $Ti_{11}Ni_{14}$ precipitates than Ni-rich TiNi binary alloys.

In alloy A, when the ageing time reaches 50 h, precipitates have grown to a critical size in which coherent stresses surround $Ti_{11}Ni_{14}$ precipitates due to the coherency boundaries existing between $Ti_{11}Ni_{14}$ precipitates and BZ matrix, as reported in 400 °C aged $Ti_{49.2}Ni_{50.8}$ alloy [15, 22]. At and after this time, the hardness increases quickly and reaches a maximum at 120 h ageing. Thereafter, the precipitates will lose their coherence and coarsen gradually when aged longer, and eventually at 400 °C × 400 h ageing, the hardness is softer than the as-solution-treated specimen. This result also implies that, in alloy A, the Al-soluted in the matrix of the 400 h aged specimen may be a little less than that of the as-solution-treated specimen.

From Fig. 5a and c, for the 400 °C × 240 h ageing, $Ti_{11}Ni_{14}$ precipitates in alloy B are greater in number and far larger in size than those in alloy A. This means that the precipitation hardening effect of the former alloy aged at 400 °C is more obvious and faster than that of the latter one, as shown in Fig. 7. The reasons for these features are that alloy B has the larger Ni/Ti ratio and the higher number of soluted Al atoms. Therefore, $Ti_{11}Ni_{14}$ nucleation and growth rates of alloy B should be different from those of alloy A. We believe that the larger Ni/Ti ratio of aged Ni-rich Ti-Ni-Al alloys can enhance $Ti_{11}Ni_{14}$ nucleation and growth rates. Conversely, the Al atoms soluted in these alloys can retard these rates, as discussed above. The more Al in solid solution in the matrix, the greater the retarding effect. These two conflicting effects cause the maximum hardness of alloy B to occur at 50 h ageing, but that of alloy A to occur at 120 h, as shown in Fig. 7.

4.3. Shape memory recovery

Fig. 8 shows the shape memory effect (SME) of alloys A and B. Comparing Fig. 8 and 7, one can find that the curve peak of SME just corresponds to that of hardness. In other words, the SME increases with increasing ageing time, reaches 100% at the peak of hardness, and then decreases with longer ageing time, The reason for this characteristic is related to the strengthening effect by the solution and precipitation hardening. The strengthening effect makes it difficult for dislocations to move and reduces the permanent strain during deformation. This phenomenon is similar to the strenghtening effect induced by cold working and thermal cycling which can improve the characteristics of pseudoelasticity and SME in TiNi alloys [20, 30]. However, the SME will decrease gradually in overaged specimens due to the reduction of the

strengthening effect. Nevertheless, Fig. 8 shows that the aged alloys A and B exhibit very good SME.

5. Conclusions

1. The transformation sequence of 400 °C aged $Ti_{49.5}Ni_{50.13}Al_{0.37}$ alloy is found to be B2↔R-phase↔B19′ martensite in the first 50 h of ageing, then to be B2↔R-phase at 120 h ageing, and then to be B2↔R-phase↔B19′ again for the further ageing. The transformation sequence of 400 °C aged $Ti_{47.5}Ni_{50.65}Al_{1.85}$ alloy shows B2↔R-phase only for an ageing time of more than 10 h. All of these characteristics are associated with the $Ti_{11}Ni_{14}$ precipitates during ageing.

2. Both solution hardening and precipitation hardening occur in $Ti_{49.5}Ni_{50.13}Al_{0.37}$ and $Ti_{47.5}Ni_{50.65}Al_{1.85}$ shape memory alloys. The hardening effects of $Ti_{47.5}Ni_{50.65}Al_{1.85}$ alloy are much higher than those of $Ti_{49.5}Ni_{50.13}Al_{0.37}$ alloy because the former alloy has the larger Ni/Ti ratio and the greater number of soluted Al atoms compared to the latter alloy. It is suggested that the larger Ni/Ti ratio can enhance the $Ti_{11}Ni_{14}$ nucleation and growth rates. However, the soluted Al atoms in the matrix can retard these rates due to the soluted Al which can affect the diffusivity of Ti and Ni atoms during the ageing process. These two conflicting effects make the Ni-rich Ti–Ni–Al alloys studied in this paper to possess different hardening effects.

3. Both $Ti_{49.5}Ni_{50.13}Al_{0.37}$ and $Ti_{47.5}Ni_{50.65}Al_{1.85}$ alloys exhibit very good shape memory effect. The maximal shape recovery effect occurs at the peak of hardness due to the strengthening effect of solution and precipitation hardening in aged specimens.

Acknowledgements

The authors are grateful to Dr T.S. Chou, Steel and Aluminum R&D Department, China Steel Corporation, for his great assistance with the internal friction measurement. Also, they would like to thank Dr C.I. Wang, Materials R&D Center, Chung-Shan Institute of Science and Technology, for his kind permission to use the Jeol-4000FX TEM. The financial support of this study by the National Science Council (NSC), Republic of China, under Grand NSC83-0405-E002-029 is also sincerely appreciated.

References

1. V. N. KHACHIN, Y. I. PASKAL, V. E. GUNTER, A. A. MONASEVICH and V. P. SIVOKHA, *Phys. Metal Metall* **46** (1978) 49.
2. K. H. ECKELMEYER, *Scripta Metall.* **10** (1976) 667.
3. J. E. HANLON, S. R . BUTLER and R. J. WASILEWSKI, *Trans. TMS-AIME* **239** (1967) 1323.
4. S. MIYAZAKI, Y. OHMI, K. OTSUKA and Y. SUZUKI, *J. Phys.* (*suppl.*) **43** (1982) C4-255.
5. W. B. CROSS, A. H. KARIOTIS and F. J. STIMLER, "Nitinol Characterization Study" (NASA.CR-1433, September 1969).
6. M. MATSUMOTO and T. HONMA "New Aspects of Martensitic Transformation" (Japan Institute of Metals, Kobe, 1976) p. 199.
7. F. E. WANG, B. F. DESAVAGE, W. J. BUEHLER and W. R. HOSLER, *J. Appl. Phys.* **39** (1968) 2166.
8. G. P. SANDROCK, A. J. PEKIN and R. F. HEHEMANN, *Metall. Trans.* **2** (1971) 2769.
9. C. M. WAYMAM, I. CONELIS and K. SHIMIZU, *Scripta Metall.* **6** (1972) 115.
10. M. NISHIDA and T. HONMA, *ibid.* **18** (1984) 1299.
11. K. IWASAKI, R. HASIGUTI, *Trans. JIM.* **28** (1987) 363.
12. M. NISHIDA and C. M. WAYMAM, *Metallography* **21** (1988) 255.
13. S. K. WU and C. M. WAYMAM, *Acta Metall.* **37** (1989) 2805.
14. S. K. WU, H. C. LIN and T. S. CHOU, *ibid.* **38** (1990) 95.
15. S. K. WU and H. C. LIN, *Scripta Metall.* **25** (1991) 1529.
16. K. R. EDMONDS and C. M. HWANG, *ibid.* **20** (1986) 733.
17. C. M. HWANG and C. M. WAYMAM, *ibid.* **17** (1983) 1344.
18. *Idem*, *Metall. Trans.* **A15** (1984) 1155.
19. Y. K. AU and C. M. WAYMAM, *Scripta Metall.* **6** (1972) 1209.
20. H. C. LIN and S. K. WU, *ibid.* **26** (1992) 59.
21. C. M. HWANG, M. MEICHLE, M. B. SALAMON and C. M. WAYMAM, *Phil. Mag.* **A47** (1983) 9.
22. H. C. LIN, PhD thesis, Institute of Materials Science and Engineering, Nation Taiwan University (1992).
23. J. S. ZHU, R. SCHALLER and W. BENOIT, *Phys. Lett. A* **141** (1989) 177.
24. M. NISHIDA, C. M. WAYMAM and T. HONMA, *Scripta Metall.* **19** (1985) 983.
25. T. TADAKI, Y. NAKATA, K. SHIMIZU and K. OTSUKA, *Trans. JIM.* **27** (1986) 731.
26. U. ZWICKER and U. J. SPIERING, *Z. Metallkd.* **64** (1973) 885.
27. C. M. JACKSON, H. J. WAGNER and R. J. WASILEWSKI, NASA-sp5110 (1972) p.69.
28. S. K. SHARMA, M.-P. MACHT and V. NAUNDORF, *J. Non-cryst. Solids* **156–158** (1993) 437.
29. R. W. CAHN and P. HASSEN, "Physical Metallurgy" (Elsevier Science Publishers B. V., North Holland and Physics Publishing, New York, 1983).
30. S. MIYAZAKI and K. OTSUKA, *Metall. Trans.* **A17** (1986) 53.

Received 19 January
and accepted 17 September 1996